Journal of Crystal Growth 490 (2018) 71–76

Contents lists available at ScienceDirect

Journal of Crystal Growth

journal homepage: www.elsevier.com/locate/crys

Effects of Ca/Sr ratio control on optical and scintillation properties of Eu-doped Li(Ca,Sr)AlF_6 single crystals

Yuui Yokota [a,*], Chieko Tanaka [b], Shunsuke Kurosawa [a,c], Akihiro Yamaji [b], Yuji Ohashi [a], Kei Kamada [a,d], Martin Nikl [e], Akira Yoshikawa [a,b,d]

[a] New Industry Creation Hatchery Center (NICHe), Tohoku University, 6-6-10, Aoba, Aramaki, Aoba-ku, Sendai, Miyagi 980-8579, Japan
[b] Institute for Materials Research, Tohoku University, 2-1-1, Katahira, Aoba-ku, Sendai, Miyagi 980-8577, Japan
[c] Department of Physics, Yamagata University, Yamagata, Kojirakawa-mach 1-4-12, Yamagata 990-8560, Japan
[d] C&A Corporation, 6-6-40, Aoba, Aramaki, Aoba-ku, Sendai, Miyagi 980-8579, Japan
[e] Institute of Physics CAS, Cukrovarnicka 10, Prague 16200, Czech Republic

ARTICLE INFO

Article history:
Available online 14 March 2018
Communicated by T. Paskova

Keywords:
A1. X-ray diffraction
A2. Growth from melt
B1. Halides
B2. Scintillator materials
B3. Scintillators

ABSTRACT

Eu-doped Li(Ca,Sr)AlF_6 [Eu:LiCSAF] single crystals with various Ca/Sr ratios were grown by the micro-pulling-down method, and their optical and scintillation properties were investigated to reveal the effects of Ca/Sr ratio on optical and scintillation properties of the Eu:LiCSAF single crystals. The Li($Ca_{1-x-y}Sr_xEu_y$)AlF_6 single crystals could be grown in $0 \le x \le 0.1$, $0.5 \le x \le 1.0$ and $y = 0.02$ while the Eu:LiCSAF crystals with $x = 0.2$, 0.25 and 0.4 included two colquiriite-type phases with different lattice parameters. The Li($Ca_{1-x-y}Sr_xEu_y$)AlF_6 single crystal with $x = 0.25$ and $y = 0.02$ showed the highest light yield under neutron irradiation.

1. Introduction

$LiCaAlF_6$ [LiCAF] and $LiSrAlF_6$ [LiSAF] with the colquiriite-type structure (space group $P\bar{3}1c$) have been investigated as a host material for neutron scintillator which can be used in neutron detectors in homeland security devices. The LiCAF and LiSAF including ^6Li have a large capture cross-sections for thermal neutrons while their sensitivities to γ-rays are low due to the relatively low effective atomic numbers and densities. Especially, Ce- and Eu-doped LiCAF [Ce:LiCAF and Eu:LiCAF], and Ce- and Eu-doped LiSAF [Ce:LiSAF and Eu:LiSAF] single crystals showed great scintillation properties and there are many previous reports [1–5]. In addition, they have no hygroscopicity and the large bulk single crystals can be grown with relative ease by the conventional growth methods such as Czochralski [Cz] method while it is difficult to make large bulk crystals of Li-glass and Eu:LiI neutron scintillators [6].

Eu:LiCAF and Eu:LiSAF single crystals demonstrated high light yield under thermal neutron irradiation and Eu2% doped-LiCAF and LiSAF single crystals showed the highest light yield in previous reports [2,7]. However, there are few reports about the solid solution of the LiCAF and LiSAF [Li(Ca,Sr)AlF_6, LiCSAF] single crystals [8]. In the previous reports for Ce-doped $(Lu,Gd)_3(Ga,Al)_5O_{12}$ and Ce-doped $Y_3(Al,Ga)_5O_{12}$, Ce-doped Li(Ca,Sr)AlF_6 and Ce-doped Li(Ca,Ba)AlF_6 single crystals, the scintillation properties were improved by optimizing the band-gap [9–13]. In addition, optical and scintillation properties of Eu:K(Ca,Sr)I_3 single crystals have been investigated in the previous report [14], and light yield and scintillation response proportionality were improved. However, there is no report about optical and scintillation properties of the Eu-doped LiCSAF single crystals. Therefore, the purpose of this study is the crystal growth of Eu:LiCSAF single crystals with various Ca/Sr ratios and investigation of their optical and scintillation properties.

2. Experimental

The Eu:LiCSAF single crystals were grown by the micro-pulling-down [μ-PD] method with a vacuum chamber which could grow a fiber fluoride single crystal using a carbon crucible with a hole at the bottom [3,15]. Starting materials, LiF (^6Li 95%, 4N), CaF_2, SrF_2, AlF_3 and EuF_3 (4N purity) powders, were mixed as nominal compositions of Li($Ca_{1-x-y}Sr_xEu_y$)AlF_6 with $x = 0$, 0.10, 0.20, 0.25, 0.40, 0.50, 0.75 and 0.98, and $y = 0.02$. The mixed powder was heated at 300 °C under vacuum ($\sim 10^{-4}$ Pa) in the chamber in the carbon crucible by radio-frequency induction heating to remove oxygen and moisture contaminations remaining on the surface of the powders, crucible, insulator and other parts of the equipment.

* Corresponding author.
E-mail address: yokota@imr.tohoku.ac.jp (Y. Yokota).

https://doi.org/10.1016/j.jcrysgro.2018.03.022
0022-0248/

The carbon crucible has a ϕ2 mm outlet at the bottom and a carbon insulator was placed around the crucible. After the baking process, the chamber was filled with high purity Ar/CF_4 mixed gas (Ar: CF_4 = 9: 1) up to ambient pressure. Then, the crucible was heated up to the melting point of the LiCSAF (766–814 °C) and the mixed powder was completely melted. The melt in the crucible was kept a little above the melting temperature for 2 h and crystal growth was performed at 0.1 mm/min growth rate using a platinum wire as a seed. The wetting nature of the Eu:LiCSAF melt during the crystal growth changed with Sr concentration: wetting angle of the Eu:LiCSAF melt on the carbon crucible became smaller with increasing Sr concentration and it was difficult to achieve a stable liquid-solid interface for Eu:LiCSAF with larger Sr concentration (x = 0.5 and 0.75). As-grown Eu:LiCSAF single crystals were cut and polished to prepare specimens for the measurements of their optical and scintillation properties. The thicknesses of the polished specimens were 1 mm. Each polished specimen was prepared from the portion between about 5 and 10 mm from the growth's initial part, situated within the transparent and crack-free part of the as-grown single crystal. The actual Eu concentration of the polished specimens is considered to be almost the same regardless of the Ca/Sr ratio. Actual Ca/Sr ratios in the grown single crystals were almost same as that of the nominal composition, and there was no segregation of Ca and Sr along the growth direction in the chemical composition analysis by an Electron Prove Micro-Analyzer [EPMA] (JEOL JXA-8530F).

Transmittance spectra of the polished specimens were measured by a spectrophotometer (JASCO V-550) in the wavelength range from 190 to 600 nm and a Si-Photodetector at the UVSOR Facility of the Institute for Molecular Science BL3B (IRD AXUV 100) in the wavelength range from 80 to 500 nm. Powder X-ray diffraction [XRD] measurements were performed to identify the phases of the grown single crystals by an X-ray diffractometer (Brucker, D8 Discover) and calculate the lattice parameters. X-ray excited radioluminescence [XRL] spectra were measured by a Charge Coupled Device [CCD] detector (ANDOR SR163) using an X-ray source (Cu-K_α, 30 kV, 30 mA).

The pulse-height spectra and decay curves of the polished specimens were investigated under neutron irradiation emitted from a ^{252}Cf source to estimate the light yield and decay time. The neutron response measurements were performed with a photomultiplier tube [PMT] (Hamamatsu R7600U-200), lead and paraffin blocks. The polished specimens were covered with a Teflon tape except for one face which was attached to the light entrance window of

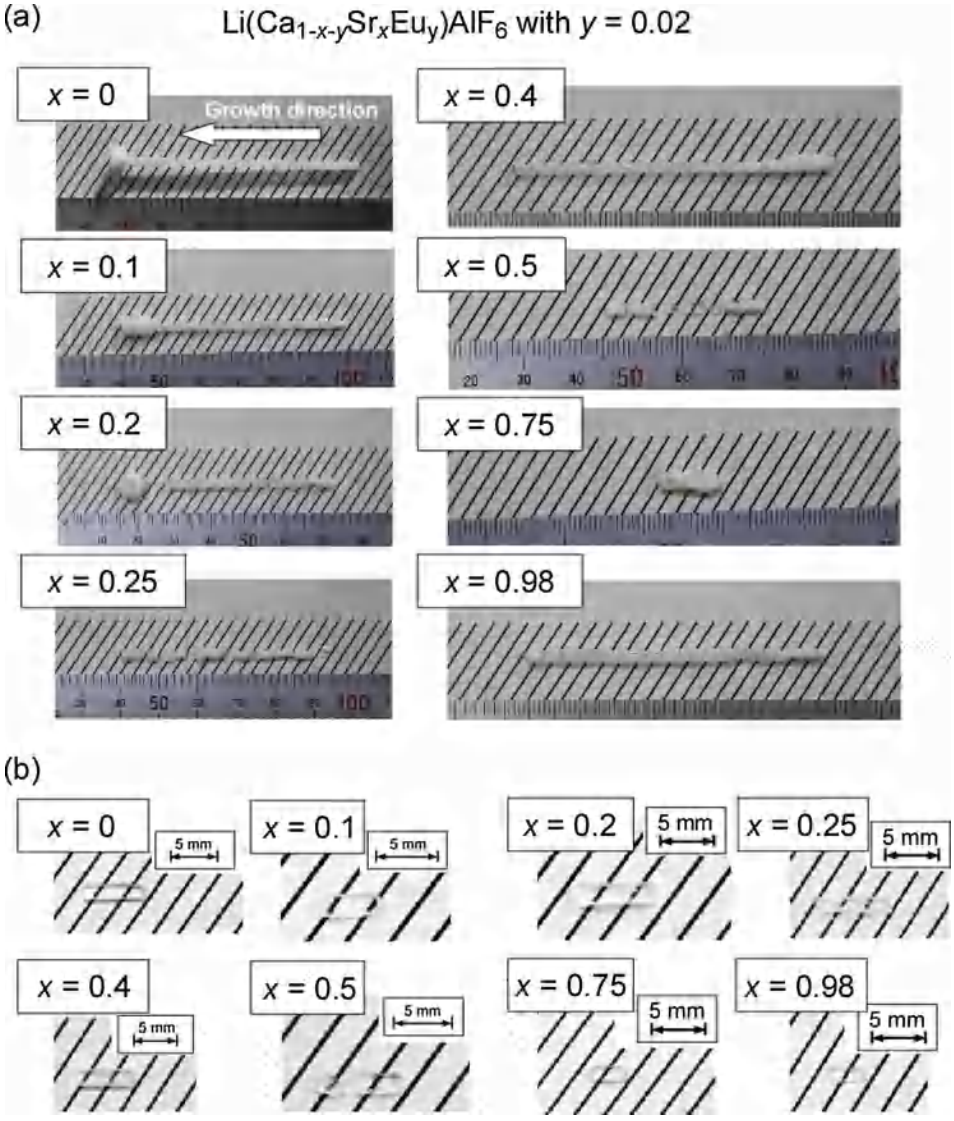

Fig. 1. (a) As-grown Eu:LiCSAF single crystals grown by the μ-PD method and (b) polished Eu:LiCSAF specimens.

the PMT with optical grease. A Li-Glass (Light yield: 6000 photons/neutron) was used as a reference to estimate the light yield by comparing peak positions in the pulse-height spectra between the Li-glass and Eu:LiCSAF single crystals. The scintillation decay curves were measured by an oscilloscope (Tectronix TDS3052B). In addition, the pulse-height spectra of the polished specimens were measured under gamma-ray irradiation emitted from a ^{60}Co source to investigate the gamma-ray responses.

3. Results and discussions

The Eu:LiCSAF single crystals with various Ca/Sr ratios were grown by the μ-PD method and are shown in Fig. 1(a). During the crystal growth, the liquid-solid interface was located just below the bottom of the crucible and the diameter of the grown single crystal was controlled by the hole (outlet). As a result, the as-grown single crystals had approximately ϕ2 mm diameter. There were some cracks around the growth's initial parts of the as-grown single crystals and the generation of cracks is due to the use of a platinum wire as the seed. The cracks gradually decreased during the crystal growth, and past about 10–60 mm from the initial end of the ingot, transparent and crack-free parts could be obtained for all Eu:LiCSAF single crystals. Specimens with 1 mm thickness were prepared from the transparent parts and the surfaces of all specimens were polished under the same conditions to evaluate the optical and scintillation properties (Fig. 1(b)). All polished specimens showed high transparency and were colorless.

Powder XRD measurements of the grown Eu:LiCSAF single crystals were performed to identify the phases and calculate the lattice parameters after parts of the single crystals were completely ground by an agate mortar. All diffraction peaks of the XRD patterns for the all Eu:LiCSAF single crystals could be identified as the colquiriite-type crystal structure (ICDF PDF77-0939) and there was no diffraction peak originated from a secondary phase except for the crystals with $x = 0.25$ and 0.75 which included the EuF_3 phase (Fig. 2(a)). However, all diffraction peaks of the Eu:LiCSAF single crystals with $x = 0.20$, 0.25 and 0.40 were split as shown in Fig. 2(b), which suggests that there are two colquiriite-type phases with different lattice parameters in those single crystals. Segregation coefficients of Eu ion in the $LiCaAlF_6$ and $LiSrAlF_6$ single crystals are extremely small due to the difference of valences between Ca (Sr) site and Eu^{3+} ion in EuF_3 [4]. Therefore, the Eu:LiCSAF single

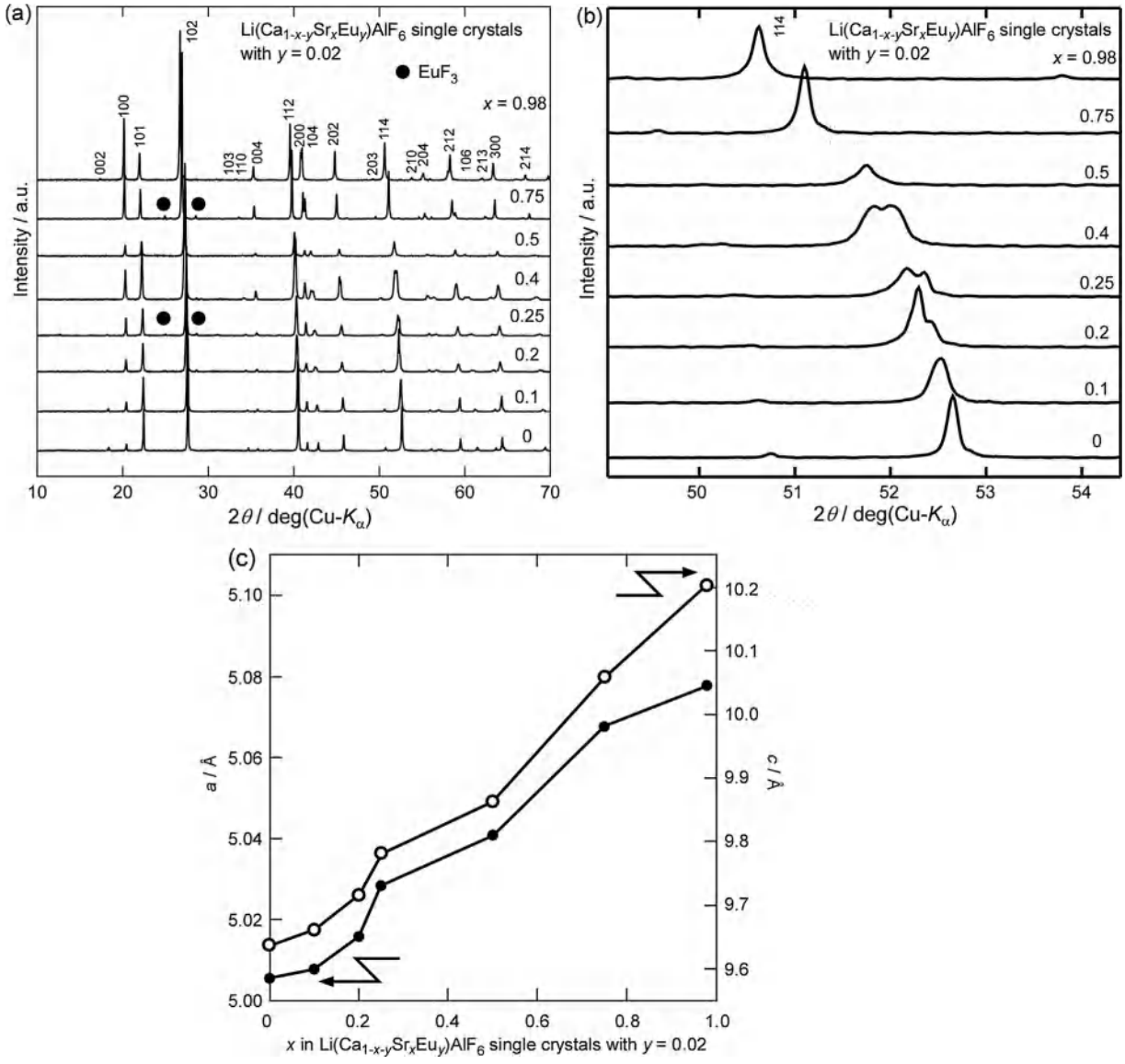

Fig. 2. (a) Powder XRD patterns, extended diffraction peaks and (b) lattice parameters of the Eu:LiCSAF single crystals.

crystals easily include the EuF_3 phase from the melt during the crystal growth, and parts included EuF_3 phase were accidentally used for the powder XRD measurements only for the Eu:LiCSAF single crystals with $x = 0.25$ and 0.75. Positions of the diffraction peaks were systematically shifted with the Sr concentration. The lattice parameters, *a*- and *c*-axes lengths, were calculated from the XRD patterns, as illustrated in Fig. 2(b). The lattice parameters were systematically increased with increasing Sr concentration and the result is attributable to the substitution of Ca^{2+} site by the Sr^{2+} ion with larger ionic radius than Ca^{2+} ion. However, the increase of lattice parameters as a function of Sr concentration doesn't fully satisfy Vegard's Law due to the generation of two phases with different lattice parameters in the *x* range of 0.2–0.4. However, the precise compositions and structures of the two phases couldn't be determined by the XRD patterns.

Transmittance spectra of the Eu:LiCSAF polished specimens were measured as shown in Fig. 3(a). Most specimens showed more than 70% transmittance in the wavelength range from 370 to 750 nm. Absorption peaks around 200 and 300 nm were observed for all specimens and they are attributable to the 4f-5d transitions of the Eu^{2+} ion. Fig. 3(b) shows the transmittance spectra of Eu:LiCSF single crystals with $x = 0$, 0.25 and 0.98 in the wavelength range from 80 to 500 nm. There was no significant difference of absorptions versus wavelength for those values of the Ca/Sr ratio. In the XRL spectra of all polished specimens (Fig. 3(c)), two emission peaks around 370 and 580 nm were observed. The emission peak around 370 nm originated from the 5d-4f transition of the Eu^{2+} ion and the wavelength of the emission peak was shifted with Sr concentration as illustrated in Fig. 3(c) and (d). The Ca/Sr-F bond length will increase with increasing Sr concentration and the $5d_1$ state will locate closer to the conduction band based on the crystal field splitting theory. As a consequence, the wavelength of the emission peak from the Eu^{2+} ion should blue-shift with increasing Sr content [16]. However, in our results, the red-shift with increasing Sr content of the emission peak from the Eu^{2+} ion was observed, and unfortunately a clear explanation of the red-shift can't be provided now. There are two previous reports related to the red-shift of the Eu^{2+} emission [17–19]. In the Eu^{2+}: $(Ba,Sr)_3Lu(PO_4)_3$ eulytite solid-solution phosphors, the red-shift of Eu^{2+} emission with increasing Ba/Sr ratio was observed and it

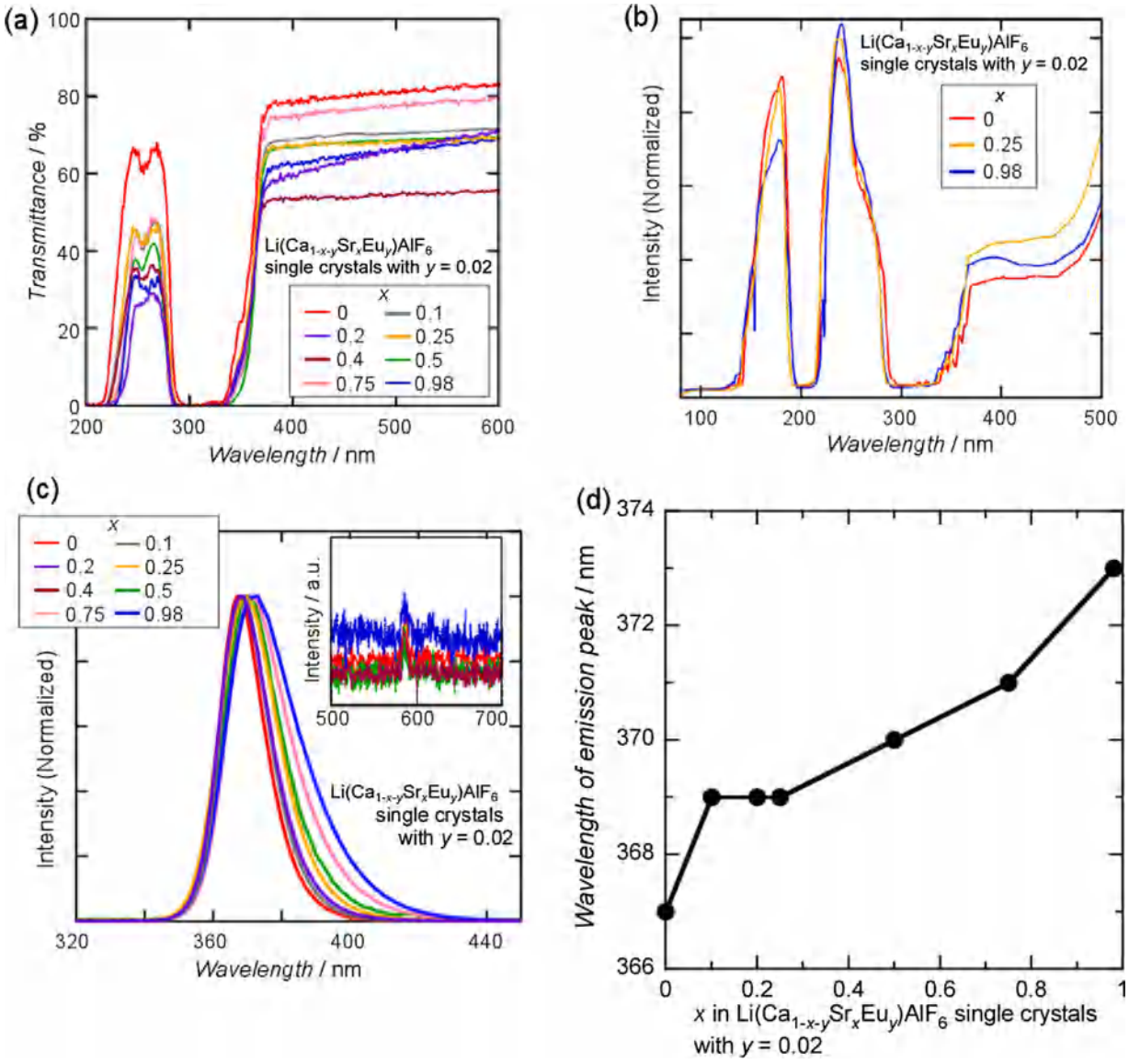

Fig. 3. (a) Transmittance spectra in the wavelength range from 190 to 600 nm and (b) from 80 to 500 nm, and (c) XRL spectra of the Eu:LiCSAF single crystals. (d) Wavelength of emission peaks of the Eu:LiCSAF single crystals.

was ascribed to weakening of the Eu^{2+} crystal field splitting from the neighboring-cation effect [17]. In addition, the red-shift with increasing Eu concentration in the Eu^{2+}:$BaGa_2S_4$ and Eu^{2+}:$CaSrSiO_4$ phosphors was observed [18,19]. However, further studies are needed to clarify the red-shift of Eu^{2+} emission. The emission peak around 580 nm is attributable to the 4f-4f transition of the Eu^{3+} ion [20–22] and there was no change of the emission wavelength. The Eu^{3+} ion originates from EuF_3 impurity or valence variation of Eu ion in Eu:LCSAF with a fluorine non-stoichiometry. The valence variation of Eu ion due to the anion non-stoichiometry was described in a previous report [23].

Pulse-height spectra and decay curves of the Eu:LiCSAF polished specimens under thermal neutron irradiation were investigated as shown in Fig. 4. All specimens showed a clear peak in the pulse-height spectra (Fig. 4(a)). However, double peaks were observed in the pulse-height spectra of the Eu:LiCSAF single crystals with $x = 0.2$, 0.25, 0.4 and 0.75, and they are attributable to two phases with different light yields in the crystals. The light yields were estimated by comparing the channels of the peaks between the Eu:LiCSAF single crystals and the Li-Glass. In addition, the pulse-height spectrum of the Eu:LiCSAF single crystal with $x = 0.4$ under gamma-ray irradiation was measured as illustrated in Fig. 4(b). A clear energy peak could be observed in the pulse-height spectrum under neutron irradiation and the neutron event could be distinguished from the gamma-ray one while the spectrum under gamma-ray irradiation slightly overlapped the range of the energy peak. The decay curves of the polished specimens under neutron irradiation are shown in Fig. 4(c). All decay curves could be fitted

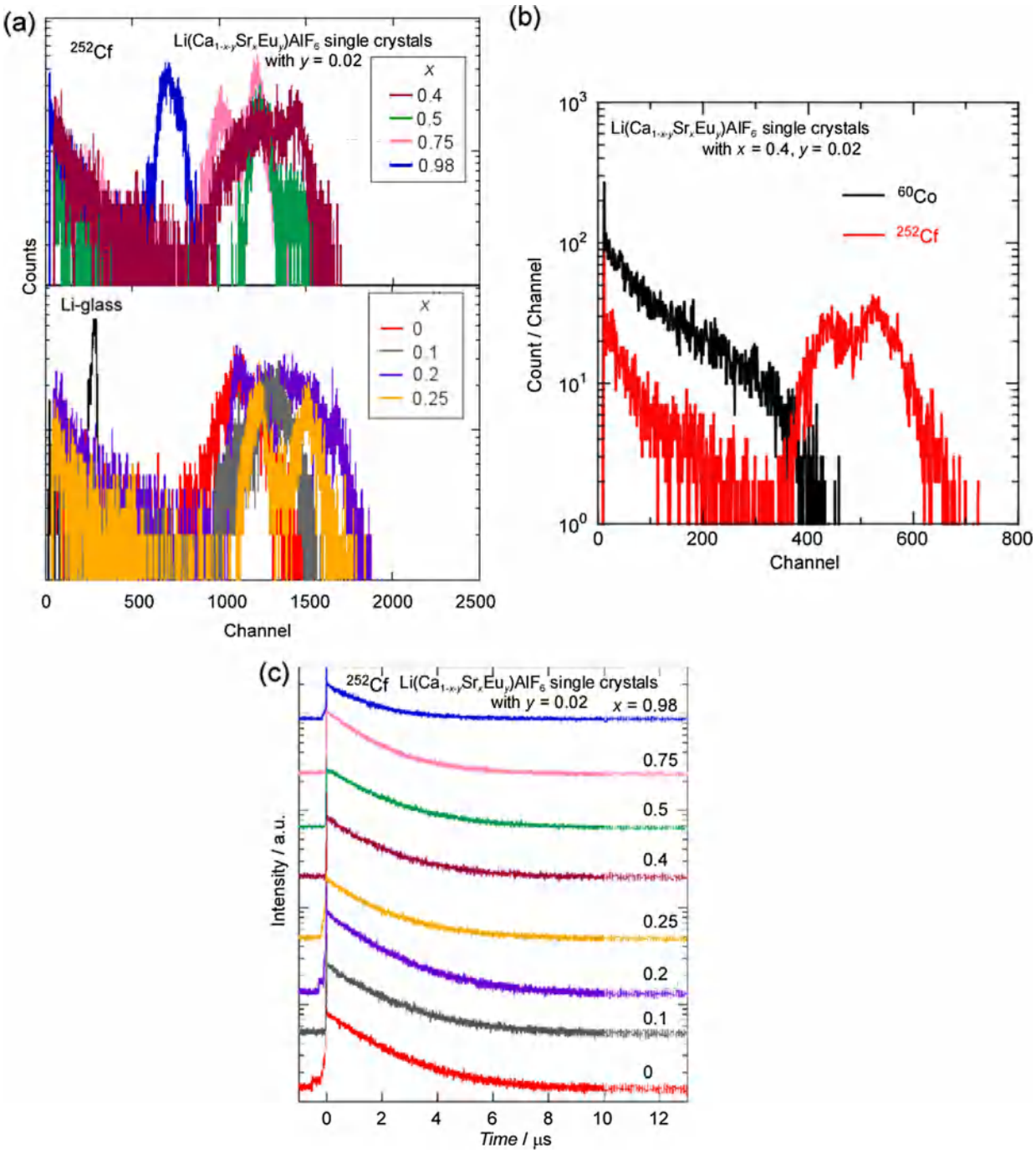

Fig. 4. (a) Pulse-height spectra and (b) decay curves of the Eu:LiCSAF single crystals under neutron irradiation.

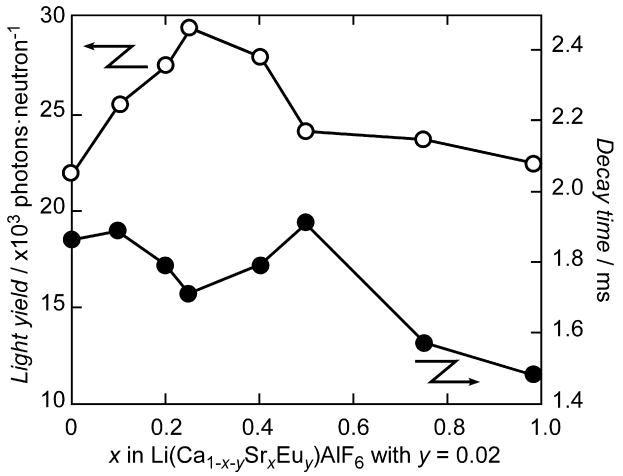

Fig. 5. Light yield and decay time of the Eu:LiCSAF single crystals under neutron irradiation.

Table 1
Scintillation properties of $Li(Ca_{1-x-y}Sr_xEu_y)AlF_6$ single crystals.

x	y	Wavelength of emission peak [nm] (5d-4f of Eu^{2+} ion)	Light yield [photons/neutron]	Decay time [μs]
0	0.02	367	21, 800	1.86
0.10	0.02	369	25, 300	1.89
0.20	0.02	369	27, 400	1.79
0.25	0.02	369	29, 300	1.71
0.40	0.02	370	27, 800	1.79
0.50	0.02	371	24, 000	1.91
0.75	0.02	373	23, 600	1.57
0.98	0.02	367	22, 300	1.48

by a single exponential decay function and decay times were estimated. The estimated light yields and decay times of the Eu:LiCSAF single crystals are described in Fig. 5 and scintillation properties of the Eu:LiCSAF were listed in Table 1. The light yields of the Eu:LiCSAF single crystals increased with increasing Sr concentration and reached the maximum light yield at $x = 0.25$. However, it is not clear which colquiriite-type phases produced the maximum light yield and further investigations are needed to determine it. Then, the light yields decreased with increasing Sr concentration in the x range from 0.25 to 1. The results suggest that the control of Ca/Sr ratio achieved a suitable band-gap for the luminescence originating from the 5d-4f transition of Eu^{2+} ion under thermal neutron irradiation. The result showed the tendency of decay times decrease with increasing Sr concentration and the decrease of the decay time is supposed to be due to the systematic change of the positional relationship between the conduction band of the LiCSAF and 5d level of Eu^{2+} ion. In a previous report [24], band-gap energies of the LiCAF and LiSAF single crystals were 12.23 and 11.79 eV, respectively and Ca/Sr sites affect the band-gap energy. This suggests that the band-gap energy of a LiCSAF single crystal decreases as the Sr/Ca ratio increases and the decrease of the band-gap energy affects the scintillation properties.

4. Conclusions

$Li(Ca_{1-x-y}Sr_xEu_y)AlF_6$ single crystals with various Sr concentrations were grown by the μ-PD method and their phases, optical and scintillation properties were investigated to reveal the effects of Ca/Sr ratio. The lattice parameters, a- and c-axes lengths, were systematically increased with increasing Sr concentration. In the XRL spectra, wavelengths of the emission peaks originated from Eu^{2+} ion systematically increased with increasing Sr concentration. The Eu:LiCSAF single crystal with $x = 0.25$ indicated the highest light yield, 29,300 photons/neutron and the result revealed that the light yield of Eu:LiCAF single crystal was improved by the adjustment of Ca/Sr ratio. In addition, the decay time showed the tendency of decrease with an increase of Sr concentration.

Acknowledgements

This work is partially supported by the Japan Society for the Promotion of Science (JSPS) Research Fellowships for Grant-in-Aid for Young Scientists (15H05551), and Czech project supporting Czech-Japan collaboration, MEYS KONTAKT II (LH14266).

References

[1] A. Yoshikawa, T. Yanagida, Y. Tokota, N. Kawaguchi, S. Ishizu, K. Fukuda, T. Suyama, K.J. Kim, J. Pejchal, M. Nikl, K. Watanabe, M. Miyake, M. Baba, K. Kamada, I.E.E.E. Trans, Nucl. Sci. 56 (2009) 3796.
[2] N.V. Shiran, A.V. Gektin, S.V. Neicheva, V.A. Kornienko, K. Shimamura, N. Ishinose, J. Lumin. 102–103 (2003) 815.
[3] Y. Yokota, Y. Fujimoto, T. Yanagida, H. Takahashi, M. Yonetani, K. Hayashi, I. Park, N. Kawaguchi, K. Fukuda, A. Yamaji, Y. Fukazawa, M. Nikl, A. Yoshikawa, Cryst. Growth Des. 11 (2011) 4775.
[4] Y. Yokota, A. Yamaji, S. Kurosawa, Y. Ohashi, K. Kamada, A. Yoshikawa, AIP Adv. 7 (2017) 125312.
[5] Y. Yokota, S. Kurosawa, K. Fukuda, K. Kamada, A. Yoshikawa, IEEE. Trans. Nucl. Sci. 61 (2013) 419.
[6] K. Shimamura, S.L. Baldochi, I.M. Ranieri, H. Sato, T. Fujita, V.L. Mazzocchi, C.B. R. Parente, C.O. Paiva-Santos, C.V. Santilli, N. Sarukura, T. Fukuda, J. Cryst. Growth 223 (2001) 383.
[7] A. Yamaji, T. Yanagida, N. Kawaguchi, Y. Fujimoto, Y. Yokota, K. Watanabe, A. Yamazaki, A. Yoshikawa, J. Pejchal, Nucl. Instr. Meth. Phys. Res. A 659 (2011) 368.
[8] Y. Yokota, A. Yamaji, S. Kurosawa, K. Kamada, A. Yoshikawa, Opt. Mater. 36 (2014) 1950.
[9] T. Yanagida, N. Kawaguchi, Y. Fujimoto, K. Fukuda, Y. Yokota, A. Yamazaki, K. Watanabe, J. Pejchal, A. Uritani, T. Iguchi, A. Yoshikawa, Opt. Mater. 33 (2011) 1243.
[10] K. Kamada, T. Endo, K. Tsutumi, T. Yanagida, Y. Fujimoto, A. Fukabori, A. Yoshikawa, J. Pejchal, M. Nikl, Cryst. Growth Des. 11 (2011) 4484.
[11] O. Sidletskiy, V. Kononets, K. Lebbou, S. Neicheva, O. Voloshina, V. Bondar, V. Baumer, K. Belikov, A. Gektin, B. Grinyov, M.-F. Joubert, Mater. Res. Bull. 47 (2012) 3249.
[12] A.A. Shavelev, A.S. Nizamutdinov, V.V. Semashko, M.A. Marisov, J. Phys. Conf. Ser. 560 (2014) 012001.
[13] Y. Yokota, S. Kurosawa, K. Fukuda, K. Kamada, A. Yoshikawa, I.E.E.E. Trans, Nucl. Sci. 61 (2014) 419.
[14] Y. Wu, Q. Li, B.C. Chakoumakos, M. Zhuravleva, A.C. Lindsey, J.A. Johnson II, L. Stand, M. Koschan, C.L. Melcher, Adv. Opt. Mater. 4 (2016) 1518.
[15] Y. Yokota, S. Kurosawa, Y. Shoji, Y. Ohashi, K. Kamada, A. Yoshikawa, Opt. Mater. 65 (2017) 46.
[16] V. Bachmann, C. Ronda, O. Oeckler, W. Schnick, A. Meijerink, Chem. Mater. 21 (2009) 316.
[17] Z. Wang, Z. Xia, M.S. Molokeev, V.V. Atuchin, Q. Liu, Dalton Trans. 43 (2014) 16800.
[18] X. Huang, J. Sun, X. Sheng, Y. Huang, L. Ning, J. Lumin. 185 (2017) 187.
[19] T. Komukai, J. Yokoyama, Y. Takatsuka, Y. Sato, H. Kato, M. Kakihana, J. Ceram. Soc. Jpn. 124 (2016) 823.
[20] N.V. Shiran, A.V. Gektin, S.V. Neicheva, V.A. Kornienko, K. Shimamura, N. Ishinose, J. Lumin. 102–103 (2003) 805.
[21] B. Dhabekar, N.S. Rawat, N. Gaikwad, S. Kadam, D.K. Koul, Radiat. Meas. 107 (2017) 7.
[22] S.R. Rahangdale, U.A. Palikundwar, S.P. Wankhede, B. Dhabekar, S. Kadam, S.V. Moharil, J. Lumin. 178 (2016) 446.
[23] B. Zhai, D. Liu, Y. He, L. Yang, Y.M. Huang, J. Lumin. 194 (2018) 485.
[24] S. Kuze, D. du Boulay, N. Ishizawa, N. Kodama, M. Yamaga, B. Henderson, J. Solid State Chem. 177 (2004) 3505.